

## An Equation for Stress Concentration Factor in Countersunk Holes

Kunigal N. Shivakumar<sup>1</sup>, Anil Bhargava<sup>1</sup> and Sameer Hamoush<sup>2</sup>

**Abstract:** A detailed three-dimensional finite element stress analysis was conducted on straight-shank and countersunk rivet holes in a plate subjected to tension loading. The study included a wide range of plate width to radius, thickness to radius, countersunk depth to thickness ratios and countersunk angles ( $\theta_c$ ). The stress concentration is maximum at or near the countersunk edge. The stress concentration depends on countersunk depth, plate thickness and width and it is nearly independent of the countersunk angle for  $80^\circ \leq \theta_c \leq 120^\circ$ . Using the finite element results and limiting conditions, an equation for stress concentration factor is developed and verified.

### 1 Introduction

Riveting is a common method of joining structural components. Joining introduces discontinuities (stress risers) in the form of holes, change in load path, and additional secondary loads such as rivet bearing and bending. Because of these, local stresses at the joint are elevated compared to structural nominal stresses. Furthermore, wherever, aero/hydro dynamic surfaces are required countersunk rivets are often used. Countersinking further complicates the stress flow and further elevates the stress concentration. These problems require a three dimensional (3-D) analysis. Accurate estimations of these local stresses are essential to predict joint strength and fatigue life.

Exhaustive studies on stress-concentration factor (SCF) in holes and notches for two-dimensional (2-D) bodies subjected to a wide variety of loadings have been reported in the literature and these results are available in handbooks. Three-dimensional (3-D) studies have also been made for plates with circular (straight-shank) holes subjected to remote tension. Folias and Wang provided a

detailed review of previous analytical solutions and presented their series solution. The Folias and Wang solution covers a wide range of ratios of hole radius to plate thickness. A detailed 3-D Finite Element Analysis (FEA) of plain (straight-shank) and countersunk hole specimens were made by Shivakumar and Newman. All these solutions were for wide plates and no width effect was included.

These studies resulted in the following conclusions for straight-shank holes.

1. Stress concentration is due to hoop stress along the bore of the hole.
2. Stress concentration depends on the dimensionless parameters ( $t/r$ ) and ( $z/t$ ), where  $z$  is the thickness co-ordinate direction and  $t$  is the plate thickness.
3. Stress concentration is highest in the mid-thickness of the plate for thin to moderately thick plates, but for thick plates, the stress concentration peaks near the free surface, (at about  $t/10$ )
4. The state-of-stress is plane strain in the central region, is plane stress at the free surface and is intermediate in the transition region. Thus, the stress flows into the central region of the plate causing higher stress concentration than at the surface.
5. The stress concentration is about 4 to 7% higher than plane stress value ( $K_t = 3$ ) and it increases with plate thickness. Plane stress value is recovered for very thin plates. The stress concentration is about 10% lower than plane stress value at the free surface.

Only few papers have been published for countersunk rivet holes that directly relate to stress concentration. The first was by Wharely in 1965 using birefringent coating on aluminum plates to measure the stresses on the surface of the plate with countersunk holes. Unfortunately, his experiment did not measure the stress concentrations

<sup>1</sup> Department of Mechanical and Chemical Engineering, Center for Composite Materials Research, North Carolina A&T State University, Greensboro, NC 27411

<sup>2</sup> Department of Civil and Architectural Engineering, Center for Composite Materials Research, North Carolina A & T State University, Greensboro, NC 27411

at the edge of the countersink, where the concentration is highest. The other experimental work was by Cheng in 1978 using stress freezing technique to obtain stress through the thickness of plate with a countersunk hole. He investigated a total of 13 configurations with different countersink angles and depths; seven specimens for tension loading and six for bending loading. Cheng's results showed conclusively that the highest stress concentration in the tension loading is at the edge of the countersink. In the early 1990's Shivakumar and Newman conducted a detailed 3-D FE analysis of countersunk holes in a wide plate subjected tension, bending and wedge loadings. Their study included a wide range of countersink depth,  $t/r$ , and a countersink angle,  $\theta_c$ . Numerical results were presented in the form of charts, tables and a simple FORTRAN program with an interpolation scheme. Their equation did not include finite width effects and lacked physical meaning of the geometric parameters of the hole. In 1993, Young and Lee conducted an independent 3-D FE analysis of plates with countersunk holes subjected to tension load. Their study included practical range of thickness, width, and countersunk depth. Using their finite element results, Young and Lee came up with a design equation for stress concentration in countersunk holes. A main difficulty in accepting Young and Lee's results is that their FE model was very coarse and the equation given does not agree with Heywood's equation for 2-D finite plate. Therefore, this study is undertaken to establish accurate SCF for countersunk holes and then to develop a more accurate physically based equation. An exhaustive 3-D FE study with very fine modeling will be conducted. The parametric study includes thickness to radius ( $t/r$ ) ratio, countersink depth to thickness ( $C_s/t$ ) ratio, plate width to radius ( $w/r$ ) ratio and countersink angles. Based on these results and limiting solutions for straight-shank hole and thin plates, an equation for SCF in countersunk hole is presented.

### Nomenclature

$b$	depth of straight-shank portion of hole
$C_s$	countersink depth ( $t - b$ )
$E$	Young's modulus
FEA	finite element analysis
$h$	one-half height of plate
$K_t$	maximum stress-concentration factor along bore of hole under tension
$K_t(z)$	stress concentration factor along bore of hole

	under tension
$r$	radius of straight-shank portion of hole
$S$	applied remote tension stress
SCF	stress concentration factor
SS	straight-shank
$t$	plate thickness
$w$	plate half-width
$x, y, z$	Cartesian coordinate system
$\nu$	Poisson's ratio
$\theta_c$	countersink angle

## 2 Rivet Hole Configurations

Figure 1 shows the configuration and nomenclature of countersunk hole in a plate of height and width  $2h$  and  $2w$ , respectively, subjected to a remote tensile stress  $S$ . The hole radius is  $r$  and the straight-shank, countersink and the total depths are  $b$ ,  $C_s$  and  $t$  respectively. The three depths are related by the equation  $t = b + C_s$ . The countersink angle is  $\theta_c$ . The parameters  $C_s$ ,  $t$ ,  $\theta_c$  can simulate all cases of hole configurations from straight-shank ( $C_s/t = 0$ ) to knife edge ( $C_s/t = 1$ ).

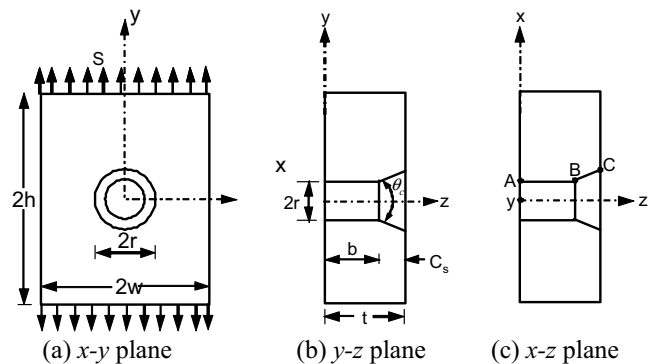


**Figure 1 :** Nomenclature, configuration and loading of a countersunk rivet hole

**Thickness to radius ( $t/r$ ) ratio:** Plate thicknesses chosen are  $0.5r$ ,  $1r$ ,  $2r$  and  $4r$  for all hole configurations and an additional  $0.4r$  and  $10r$  are included for straight-shank holes. Thickness cases  $0.5r$  to  $2r$  represent aircraft structural joints and  $4r$  and higher represent marine structures.

**Countersunk angle ( $\theta_c$ ):** Commonly used countersink angle is  $100^\circ$ . However a range of  $\theta_c$  from  $60^\circ$  to  $120^\circ$  were included to evaluate the effect of countersink angle.

**Countersink depth ( $C_s$ ):** Countersink depth is expressed as a ratio of countersink depth to plate thickness. The  $C_s$  values chosen are 0 (straight-shank hole), 0.25t,

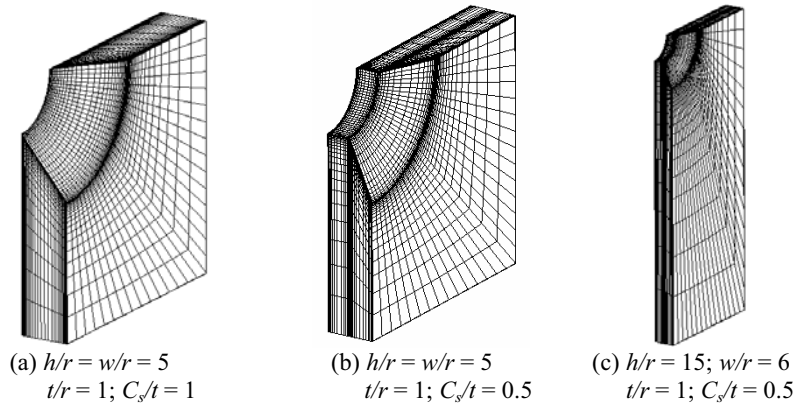


**Figure 2** : Finite element models of three countersunk rivet hole configuration

0.5t, 0.75t and 1.0t. The case  $C_s = t$  represents the knife edge, which can occur due to poor control of drilling holes.

**Plate width to radius ratio:** First, a wide plate case is studied with half-width to radius ratio ( $w/r$ ) of 15 and then  $w = 2r, 3r, 4r, 5r$  and  $6r$  are chosen to evaluate the width effect. The later cases represent the practical cases in structural applications. In addition, some specific cases are considered to verify the finite element model; those specific cases will be listed as and when they appear.

### 3 Definition of Stress-Concentration Factor

Although the definition of the stress-concentration factor is given in many classical books on theory of elasticity and in stress-concentration handbooks, many of these solutions are for 2-D configurations. For 3-D configurations, the stress concentration varies along the bore of the hole. The stress-concentration factor is defined as a function of  $z$  coordinate along the line formed by the intersection of  $y=0$  plane and the hole. The line connecting the points A, B, C in Figure 1(c) defines the path of interest. Thus,  $K_t(z)$  is the ratio of hoop stress  $\sigma_{yy}$  along the line A-B-C and the remote stress  $S$ ,  $K_t(z) = \sigma_{yy}(z)/S$ . The stress concentration factor  $K_t$  is the maximum of  $K_t(z)$ .

### 4 Finite-Element Analysis

A three-dimensional finite-element analysis (FEA) is conducted using a commercial code ANSYS version 8.1 with the 8-noded hexahedron element SOLID45. The material property used is  $E = 10E6$  and  $\nu = 0.3$ . Note that any finite value of  $E$  is acceptable because the SCF

does not depend on the material property for isotropic plates. Because all configurations considered are symmetric about  $x=0$  and  $y=0$  planes, only one quarter of the geometry is modeled by imposing symmetry conditions and a node at ( $x=z=0$  and  $y=r$ ) restrained against  $z$ -deformation. The FE idealization is made by using finer mesh in the stress gradient region and coarser mesh at the low or no stress gradient regions. Typical mesh for configurations  $h/r = w/r$  (Figs. 2a and 2b) and narrow width (Fig. 2c) plates are shown in Figure 2. Stress analysis is conducted for remote stress of  $S = 1$ , deformation and stress field are examined, and the hoop stress along the nodal line A-B-C are extracted. These stresses directly give the stress concentration  $K_t(z)$ .

An exhaustive comparison of present FE results and published data and the mesh convergence study are made in another paper and found that the present models and results are indeed accurate. In the interest of the length of the paper those results are not presented here.

### 5 Finite-Element Results

Finite element analysis is conducted for a wide range of  $\theta_c$ ,  $C_s/t$ ,  $t/r$ , and  $w/r$  values keeping the loading as far as possible from the hole by selecting  $h/r = 15$ . These results are summarized. First, wide plate ( $w/r = 15$ ) results are presented and then the results for finite width plate are presented.

**Effect of countersink angle ( $\theta_c$ ):** Figure 3 shows variation of  $K_t(z)$  along  $z/t$  for  $\theta_c$  values ranging from  $60^\circ$  to  $120^\circ$  including the results for  $\theta_c = 100^\circ$  (typical countersink angle in aircraft structures) for  $h/r = w/r = 15$ ,  $t/r = 1$  and  $C_s/t = 0.25$ . The stress concentration for  $\theta_c = 100^\circ$

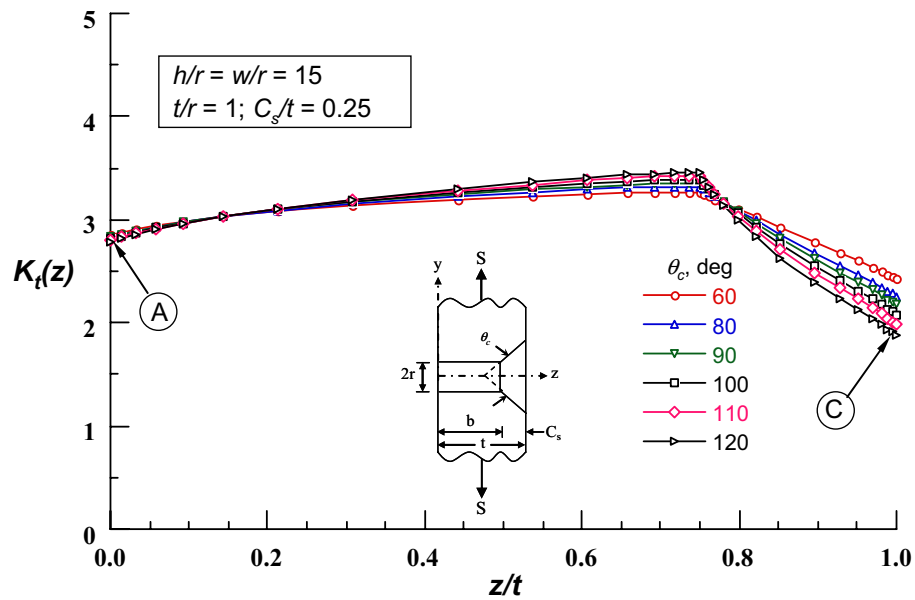


Figure 3 : Effect of countersink angle  $\theta_c$  on  $K_t(z)$  for a wide plate

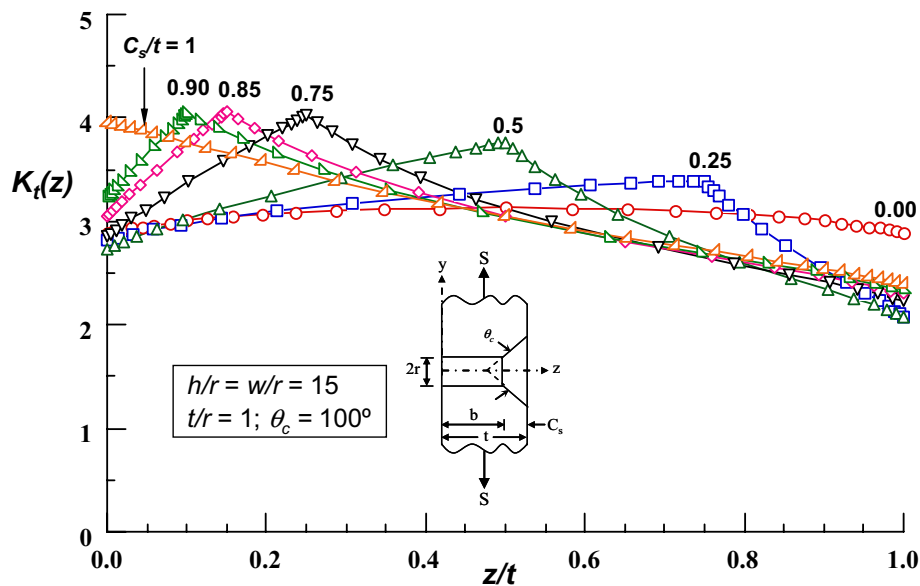


Figure 4 : Effect of countersunk depth on stress concentration distribution for a wide plate

is considered as the base line for all comparisons.  $K_t(z)$  is maximum at the countersink (B) and it drops off towards the free surfaces. Furthermore,  $K_t(z)$  at C is lower than that at A. The maximum SCF ( $K_t$ ) increased with  $\theta_c$  and this trend continued beyond  $120^\circ$ . This trend is in contradiction with Young and Lee's FE results and their hypothesis. The reason for monotonic increase in  $K_t$  with  $\theta_c$  is due to continued channeling of load path to the countersink edge and around the hole. More details

of this study are presented in ref.12. However,  $\theta_c = 180^\circ$  is a special case and at this angle the stress distribution is same as that of the straight-shank hole. The  $K_t$  difference between  $\theta_c = 90^\circ$  and  $100^\circ$  and between  $\theta_c = 100^\circ$  and  $110^\circ$  is about 1%, therefore the variation of  $K_t$  for a small deviation of  $\theta_c$  from  $100^\circ$  can be neglected. Furthermore,  $K_t$  for  $\theta_c = 80^\circ, 100^\circ$  and  $120^\circ$  are 3.33, 3.38 and 3.45 respectively. Variation of  $K_t$  from  $\theta_c = 100^\circ$  for these extreme angles is still less than 2%. The remaining

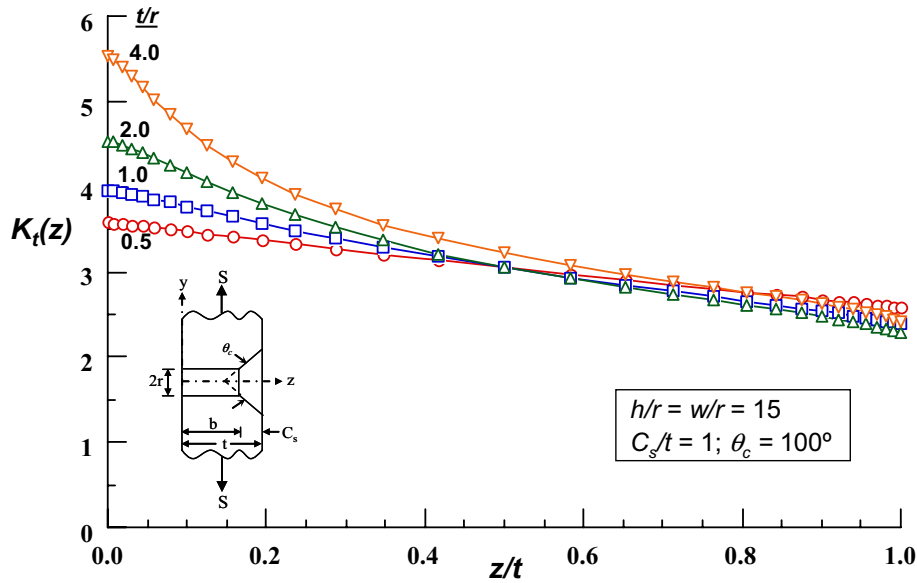


Figure 5 : Effect of  $t/r$  on stress concentration distribution for a knife-edge countersink

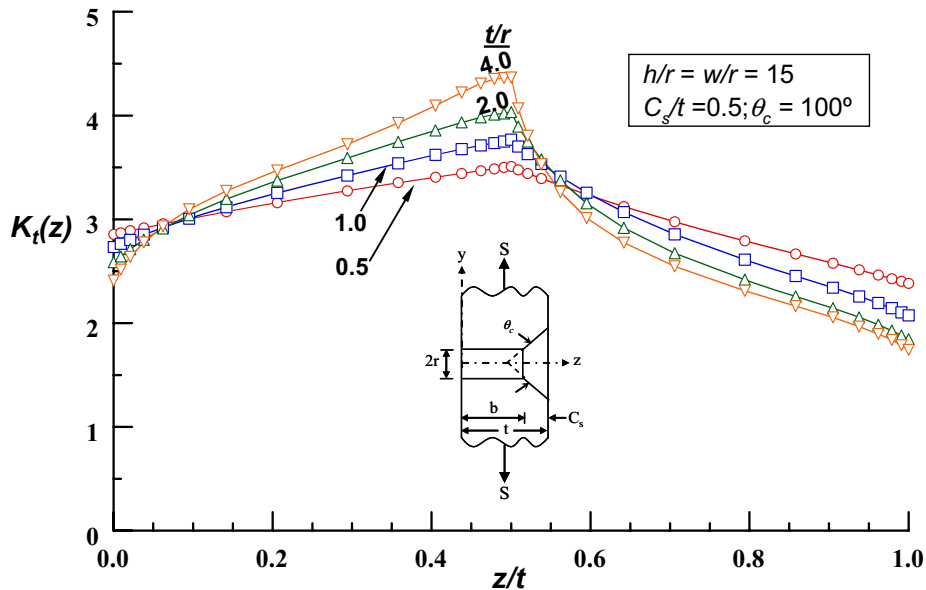


Figure 6 : Effect of  $t/r$  on stress concentration distribution for  $C_s/t = 0.5$

analyses are conducted for  $\theta_c = 100^\circ$ , baseline condition. **Effect of countersink depth ( $C_s/t$ ):** Figure 4 shows variation of  $K_t(z)$  along  $z/t$  for different depths of countersink for  $t/r = 1$ . Maximum SCF ( $K_t$ ) increased with countersink depth but decreased for the knife edge case ( $C_s/t = 1$ ). This trend is similar to Shivakumar and Newman and Young and Lee’s FE results. However, this trend is also a function of  $t/r$ . In general, maximum SCF occurs at the countersunk edge, but for shallow countersinks (see for  $C_s/t = 0.25$ ) and thick plates ( $t/r \geq 1$ ), it

occurs slightly away (5% of  $t$ ) and towards the SS of the hole.

**Effect of thickness to radius ratio ( $t/r$ ):** Figures 5 and 6 show the effect of  $t/r$  on  $K_t(z)$  for  $C_s/t = 1$  and  $0.5$ . Values of  $t/r = 0.5, 1$  and  $2$  represent the practical range of hole configurations used in aircraft industries and  $t/r > 2$  is for thick structures, for example marine industries. The  $K_t$  increased monotonically with  $t/r$  and it is consistent for all cases of  $C_s/t$  (other cases are not shown). The  $K_t$  values for different  $C_s/t$  and  $t/r$  values with  $w/r = h/r =$

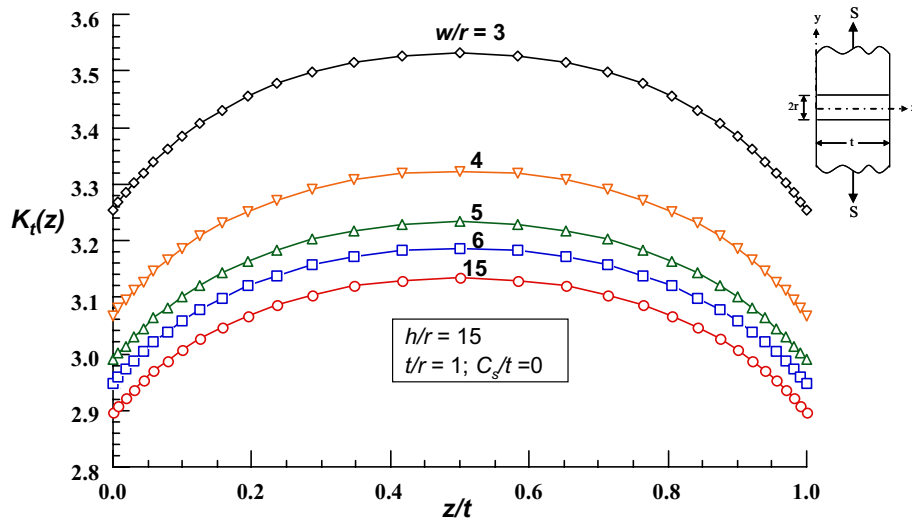


Figure 7 : Effect of  $w/r$  on stress concentration distribution

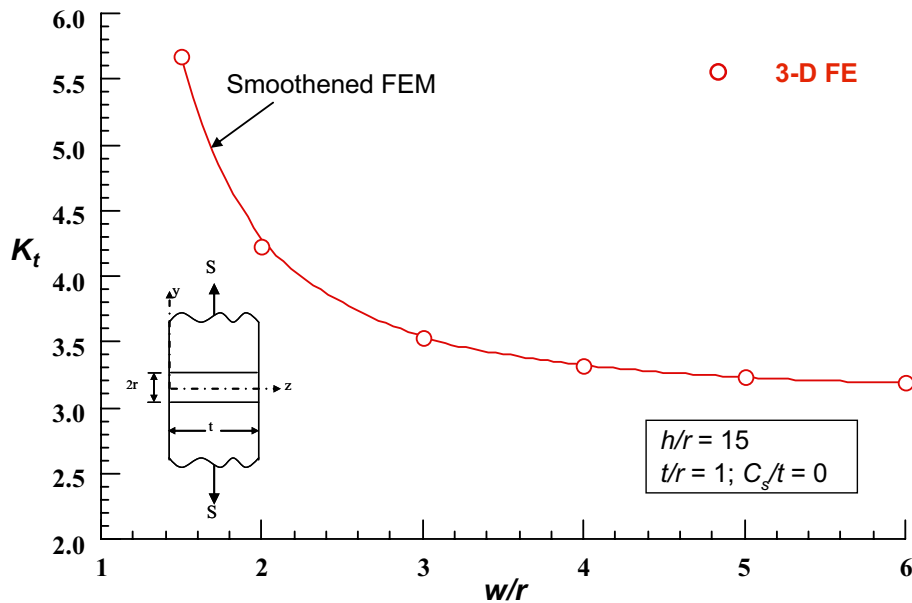


Figure 8 : Effect of  $w/r$  on stress concentration  $K_t$  for a straight-shank hole

15 and  $\theta_c = 100^\circ$  are listed in Table 1.

Table 1 : Stress concentration  $K_t$  ( $w/r = h/r = 15$ )

$C_s/t$	$t/r$ values				
	0.00	0.50	1.00	2.00	4.00
0.00	3.00	3.083	3.134	3.183	3.160
0.25	3.00	3.261	3.384	3.526	3.711
0.50	3.00	3.510	3.767	4.036	4.368
0.75	3.00	3.616	4.026	4.526	5.095
0.85	3.00	-	4.056	-	-
0.90	3.00	-	4.040	-	-
1.00	3.00	3.580	3.952	4.533	5.530

**Effect of plate width to radius ratio ( $w/r$ ):** Plate width to hole radius ratio effect is studied through analyzing configurations of different  $C_s/t$  and  $w/r$  ratios. Chosen values of  $C_s/t$  are 0, 0.25, 0.5, 0.75 and 1.0 and  $w/r$  are 3, 4, 5, 6 and 15. For straight-shank hole,  $w/r$  of 1.5 and 2 are also chosen. In all cases  $K_t$  increased with decreased  $w/r$  values. Figure 7 shows  $K_t(z)$  distribution for straight-shank holes.  $K_t(z)$  is maximum in the central region and drops off towards the free surfaces. The free edge phenomenon which resulted due to finite value of Poisson’s ratio ( $\nu \neq 0$ ) has been very well explained by Sternberg and Sadowsky for holes and by Shivakumar

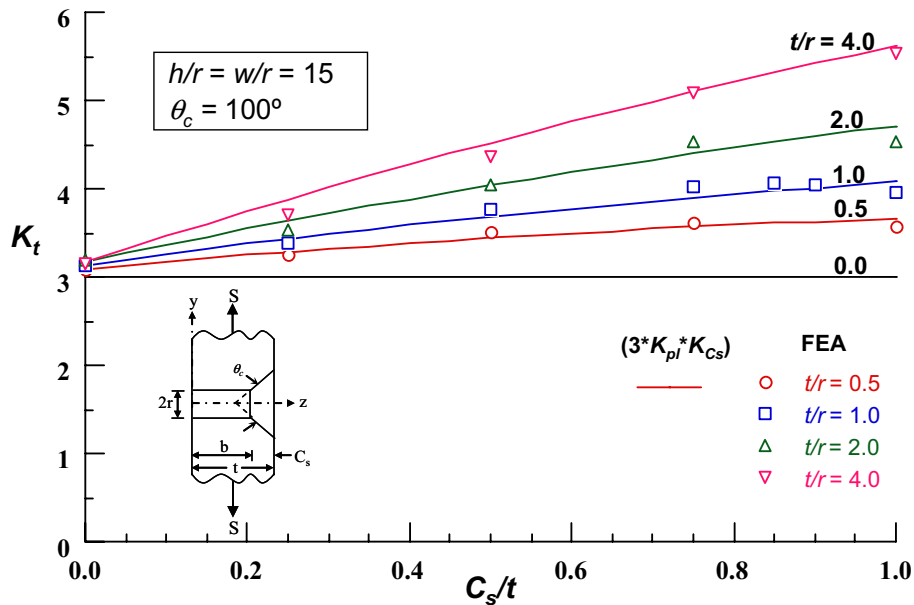


Figure 9 : Comparison of 3-D stress concentration factor equation (thickness and countersink effect) with FEA results

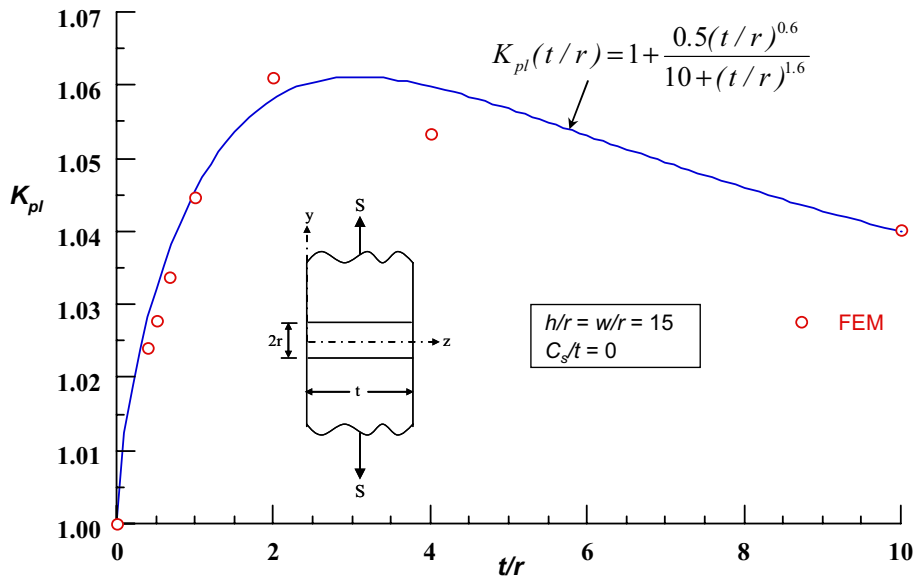


Figure 10 : 3-D stress concentration factor for a straight-shank hole (wide plate)

and Raju for cracks in solids. The straight-shank hole  $K_t$  distribution as a function of  $w/r$  is shown in Figure 8 for  $h/r = 15$  and  $t/r = 1$ . The  $K_t$  rapidly increases for smaller values of  $w/r$  and become infinite for  $w/r = 1$  as explained by Heywood for 2-D problems. For large values of  $(w/r)$ ,  $K_t$  asymptotically reaches the infinite plate solution ( $K_t = 3$ ). Heywood's equation was verified separately by 2-D FE analysis and the two solutions agreed

within 1% and these results are presented later.

### 6 Equation for Stress Concentration Factor ( $K_t$ )

While discussing the FE results in the previous sections, the  $K_t(z)$  function was used, from now the focus will be confined to the maximum of  $K_t(z)$  that is the stress concentration factor  $K_t$ . As explained,  $K_t$  occurs at countersink or very near the countersink. List of  $K_t$  for var-

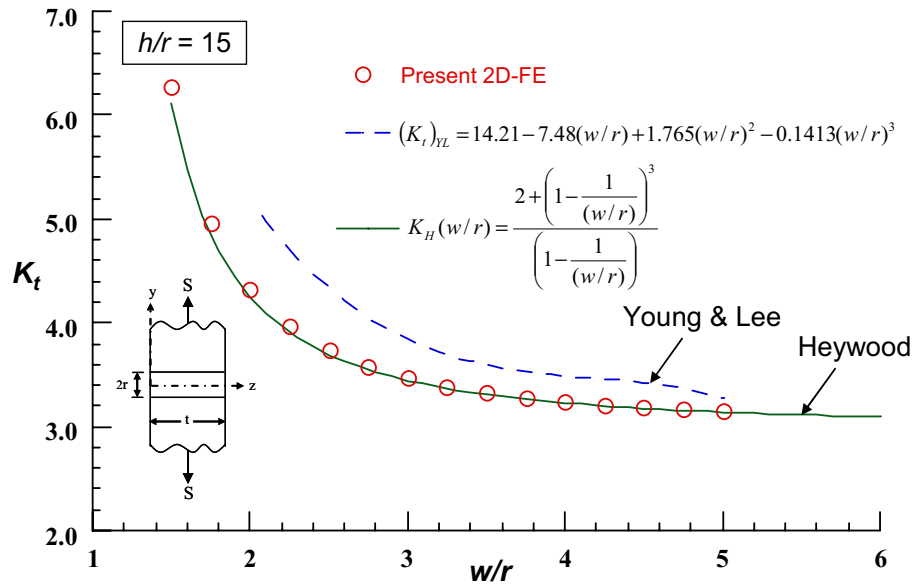


Figure 11 : Comparison of stress concentration factor for finite width plate from different analyses (2-D)

ious values of  $C_s/t$  and  $t/r$  in a wide plate ( $w/r = h/r = 15$ ) are listed in Table 1. The table includes the limiting value of  $K_t (=3)$  for  $t/r \rightarrow 0$ . Graphical representation of this data is shown in Figure 9 by symbols (FE values). To develop a  $K_t$  equation,  $K_t$  is represented as a product of three functions, namely,  $t/r$  function derived from straight-shank hole data,  $C_s/t$  function derived from countersunk data and  $w/r$  function derived from  $w/r$  data. Because  $K_t$  equation must reduce to 3 for  $t/r = 0$  for any wide plate and any  $C_s/t$ , the parameters  $t/r$  and  $C_s/t$  may not be separable. Therefore,  $K_t$  is written as:

$$K_t = K_{pl} \left( \frac{t}{r} \right) K_{Cs} \left( \frac{C_s}{t}, \frac{t}{r} \right) K_H \left( \frac{w}{r} \right) \tag{1}$$

The three functions  $K_{pl}$ ,  $K_{Cs}$  and  $K_H$ , are established for three different conditions and a combined equation is verified for finite width countersunk holes.

First  $K_{pl}(t/r)$  equation fit is performed for  $C_s/t = 0$  by using data in Table 1 and normalized by 3 (2-D  $K_t$ ). Form of the  $K_{pl}$  function is chosen such that it satisfies the limiting conditions that  $K_{pl} = 1$  for  $t/r \rightarrow 0$  (plane-stress) as well as  $t/r \rightarrow \infty$  (plane strain). This fit resulted in

$$K_{pl} \left( \frac{t}{r} \right) = 1 + \frac{0.5 \left( \frac{t}{r} \right)^{0.6}}{10 + \left( \frac{t}{r} \right)^{1.6}} \tag{2}$$

This equation agreed with 3-D FE results of SS holes within 0.5% and the correlation factor of the fit is bet-

ter than 0.98. Comparison of the equation with the FE results is shown in Figure 10.

Next, the  $K_t$  results for wide plate in Table 1 are normalized by  $C_s/t = 0$  data. The resulting values are used to perform multi-parameter fit ( $t/r$  and  $C_s/t$ ) to obtain the  $K_{Cs}$  equation. The resulting equation is:

$$K_{Cs} \left( \frac{C_s}{t}, \frac{t}{r} \right) = 1 + 0.4 \left( \frac{C_s}{t} \right) \left( \frac{t}{r} \right)^{0.6} - 0.1 \left( \frac{C_s}{t} \right)^2 \left( \frac{t}{r} \right)^{0.3} \tag{3}$$

Correlation factor of this equation is better than 0.99. Figure 9 compares the equation  $K_t = 3 * K_{pl} * K_{Cs}$  with the FE data in Table 1 for different values of  $C_s/t$  and  $t/r$ . The broken lines represent the equation and the symbols represent the FE data. The maximum difference between the equation and the data is about 3%. Thus  $K_{Cs}$  equation is sufficiently accurate for design applications.

The last equation is the width correction,  $K_H(w/r)$ . In this case, the Heywood's 2-D width correction equation is used, the subscript  $H$  represents Heywood's name. This equation was verified separately by 2-D FE analysis and the results are presented in Figure 11.

$$K_H \left( \frac{w}{r} \right) = \frac{2 + \left( 1 - \frac{r}{w} \right)^3}{\left( 1 - \frac{r}{w} \right)} \tag{4}$$

Figure 11 compares the 2-D FE results and Young and Lee's 2-D design equation  $(K_t)_{YL}$  with Heywood's equa-

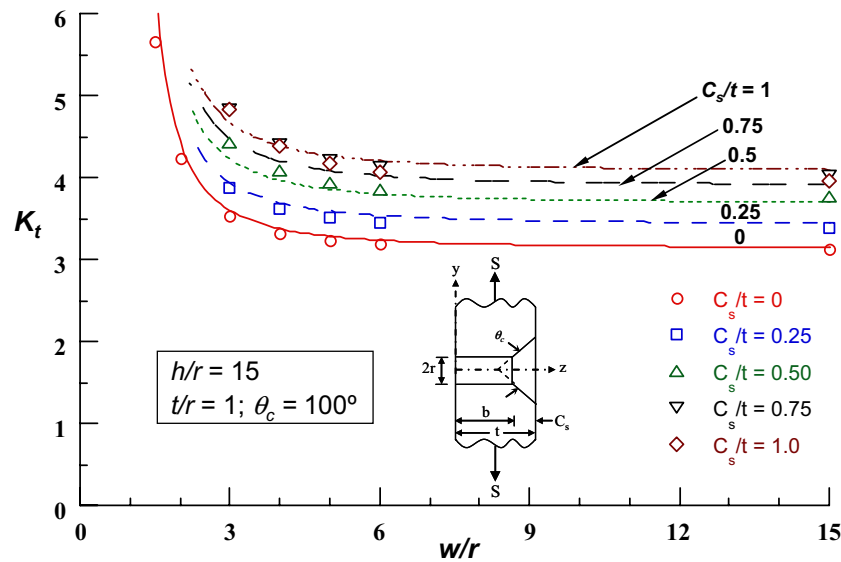


**Figure 12** : Comparison of present equation with other countersink configuration FE results

tion (4). The Heywood's  $K_H$  equation agreed within 1% of the FE results. Young & Lee's equation is not valid outside  $2 \leq w/r \leq 5$  and it over estimates stress concentration in excess of 10% for all values of  $w/r$ .

The resulting  $K_t$  equation (1) with the associated functions in equations 2, 3, and 4, is compared with the FE results for finite width plate ( $C_s/t = 0.25, 0.5, 0.75, 1.0$ ) in Figure 12. Lines represent Eq. 1 and the symbol represents FE results generated separately and not used in fitting the equation (except the data for  $w/r = 15$ ). The equation agreed with FE results very well for all ( $w/r$ ). The maximum error is about 7% for  $w/r = 3, t/r = 1$  and  $C_s/t = 0.75$ , but less than 5% for all other cases.

In summary the stress concentration equation (1) is general, accurate and satisfies all limiting cases. The equation is valid for straight-shank, countersunk including knife edge holes and for a wide range of plate sizes.

## 7 Conclusions

A detailed three-dimensional finite element stress analysis was conducted on straight-shank and countersunk rivet holes in a plate subjected to tension loading. The study included a wide range of plate widths, thicknesses, countersunk depths and countersunk angles. Results confirmed the previous result that highest stress concentration occurs at the countersink except for thick plates. For thick plates, the highest stress concentration is near the countersink and on the straight-shank

part of the hole. The stress concentration depends on countersunk depth, plate thickness and width to radius ratios. Stress concentration variation for practical range of countersunk angle ( $80^\circ$  to  $120^\circ$ ) is small (less than 2%) and therefore its effect can be neglected. Using the numerical results and limiting conditions, developed a stress concentration equation,  $K_t = K_{pl} * K_{Cs} * K_H$ ; where,  $K_{pl} = 1 + \{0.5(t/r)^{0.6} / [10 + (t/r)^{1.6}]\}$ ,  $K_{Cs} = 1 + 0.4(C_s/t)(t/r)^{0.6} - 0.1(C_s/t)^2(t/r)^{0.3}$ ,  $K_H = \{2 + [1 - 1/(w/r)]^3\} / \{1 - 1/(w/r)\}$ . This equation is accurate within 5% of finite element data for a wide range of widths, countersunk depths and plate thicknesses. The maximum error is about 7% for  $w/r = 3, t/r = 1$  and  $C_s/t = 0.75$ , but less than 5% for all other cases. In summary the stress concentration equation (1) is general, accurate and satisfies all limiting cases. The equation is valid for straight-shank, countersunk including knife edge holes and for a wide range of plate sizes.

**Acknowledgement:** The authors wish to thank Dr. Rajapakse and the Office of Naval Research through the grant no. N 00014-01-1033 and the Federal Aviation Administration (through Iowa State) through the contract no. DTFA03-98-D-0008 for their support. This paper was presented in a special session organized in the honor of 60<sup>th</sup> birthday of Prof. Satya Atluri at the ICCES/05 conference, Chennai, India, Dec 1-6, 2005

**References**

**Peterson, R. E.** (1974): *Stress Concentration Factors - Charts and Relations Useful in Making Strength Calculations for Machine Parts and Structural Elements*. John Wiley & Sons, Inc.

**Savin, G. N. (Eugene Gros, transi.)** (1961): *Stress Concentration Around Holes*. Pergamon Press, Inc.

**Green, A. E.** (1948): Three-Dimensional Stress Systems in Isotropic Plates. I. *Trans. Royal Soc. London, ser. A*, vol. 240, pp. 561-597.

**Neuber, H.** (1946): *Theory of Notch Stresses: Principles for Exact Stress Calculation*. J. W. Edwards (Ann Arbor, Michigan).

**Sternberg, E. and Sadowsky, M. A.** (1949): Three-Dimensional Solution for the Stress Concentration Around a Circular Hole in a Plate of Arbitrary Thickness. *J. Appl. Mech.*, vol. 16, no. 1, pp. 27-38.

**Folias, E. S. and Wang, J. J.** (1990): On the Three-Dimensional Stress Field Around a Circular Hole in a Plate of Arbitrary Thickness. *Comput. Mech.*, vol. 6, no. 3, pp. 379-391.

**Shivakumar, K. N. and Newman, J. C., Jr.** (1992): Three-Dimensional Stress Concentration Factor in Straight Shank and Countersunk Rivet Holes in Plates Subjected to Various Loading Conditions, *NASA TP 3192*.

**Shivakumar, K. N. and Newman, J. C., Jr.** (1995): Three-Dimensional Stress Concentration Equations for Straight-Shank and Countersunk Rivet Holes in Plates Subjected to Various Loading Conditions. *Jl. Applied Mechanics, Trans. of ASME*, vol. 62, pp. 248-249.

**Wharley, R. E.** (1965): Stress-Concentration Factors for Countersunk Holes. *Exp. Mech.*, vol. 5, no. 8, pp. 257-261.

**Cheng, Y. F.** (1978): Stress-Concentration Factors for a Countersunk Hole in a Flat Bar in Tension and Transverse Bending. *J. Appl. Mech.*, vol. 45, no. 4, pp. 929-932.

**Young, J. B. and Lee, K. K.** (1993): Stress concentration factors in countersunk holes. *Aeronautical J*, pp. 267-276.

**Bhargava, A. and Shivakumar, K. N.** (2006): Stress analysis of countersunk holes in plates subjected to tensile load. *Journal of Computers and Structures* (To be published)

**Shivakumar, K. N. and Raju, I. S.** (1990): Treatment of Singularities in Cracked Bodies. *Int. J. Fract.*, vol. 45, no. 3, pp. 159-178.